Preferential etching of metallic single-walled carbon nanotubes with small diameter by fluorine gas

Cheol-Min Yang,[1] Kay Hyeok An,[1] Jin Sung Park,[1] Kyung Ah Park,[1] Seong Chu Lim,[1] Se-Ho Cho,[2] Young Seak Lee,[3] Wanjun Park,[4] Chong Yun Park,[1] and Young Hee Lee[1,*]

[1]*BK21 Physics Division, Institute of Basic Science, Center for Nanotubes and Nanostructured Composites, Sungkyunkwan University, Suwon 440-746, Republic of Korea*

[2]*Department of Chemical Engineering, Sunchon National University, Sunchon 540-742, Republic of Korea*

[3]*Department of Fine Chemical Engineering and Chemistry, Chungnam National University, Daejeon 305-764, Republic of Korea*

[4]*Samsung Advanced Institute of Technology, Suwon 440-600, Republic of Korea*

(Received 22 August 2005; published 14 February 2006)

We have introduced a new approach to selectively remove metallic single-walled carbon nanotubes (SWCNTs) using a gas phase reaction by fluorine gas, followed by a heat treatment. The metallicity of the treated samples was characterized by the resonant Raman spectra with three wavelengths of 514, 633, and 785 nm and UV-visible-NIR absorption spectra. Peaks of metallic SWCNTs with small diameters less than 1.1 nm in the radial breathing mode of Raman spectra were greatly suppressed with fluorination and completely disappeared after heat treatment. On the other hand, the semiconducting SWCNTs with small diameters less than 1.1 nm were still retained after fluorination. Moreover, the D-band decreased after annealing at 900 °C, which was associated with the release of fluorine atoms during heat treatment. The removal of metallic SWCNTs was not observed at SWCNTs with diameters greater than 1.1 nm. The absorption data also demonstrated the similar diameter dependence in the selectivity to the Raman spectra.

DOI: 10.1103/PhysRevB.73.075419 PACS number(s): 73.22.−f, 61.46.−w, 78.67.Ch, 81.07.De

I. INTRODUCTION

Carbon nanotubes have played an important role in leading the nanoscience and nanotechnology due to their peculiar one-dimensional characteristics and potential applicabilities in various areas such as field emission displays, electron amplifiers, light bulb, hydrogen storage, fuel cell, secondary battery, supercapacitor, and nanocomposites. One important feature is its peculiar electronic structure that can be metallic and semiconducting depending on the chirality and diameter of nanotubes.[1,2] Up to now, it has not been possible to control the chirality of nanotubes systematically by the conventional synthesis approaches such as arc discharge,[3,4] laser ablation,[5] and (high-pressure) chemical vapor deposition methods.[6] Both metallic and semiconducting nanotubes coexist in the grown sample, which often hinders device applications with high performance. For instance, application to nanoscale transistors and memories requires nanotubes to be semiconducting for clear gate modulation.[7] Therefore, a selective separation of chirality is highly desired if possible.

Recently, several methods have been suggested for a selective separation of chirality. Dispersion of single-walled carbon nanotubes (SWCNTs) with octadecylamine (ODA) in tetrahydrofuran solvent leads to a reorganization of the ODA along the SWCNT sidewalls, where the amine groups prefer to physisorb on semiconducting (*s*-) SWCNTs.[8] The ac dielectrophoresis has been introduced to choose selectively metallic (*m*-) SWCNTs on the biased electrodes, whereas the *s*-SWCNTs were repelled due to the different dielectric constants between environmental solvent and nanotubes.[9] Wrapping of SWCNTs by the single-stranded DNA was also found to be sequence-dependent, where the electrostatics of the DNA-SWCNT hybrid depend on tube diameters and electronic properties, enabling nanotube separation by anion exchange chromatography.[10] A derivatized porphyrin has been also introduced to selectively interact with *s*-SWCNTs in chloroform.[11] Recently, nitronium ions (NO_2^+) were demonstrated to attack selectively small-diameter *m*-SWCNTs.[12,13] All these reactions were done in liquid phase. An idea of removing *s*-SWCNTs by a selective adsorption of carbon dioxide gas at the nanotube edges has been also suggested theoretically.[14] Our aim is to search for a simple gas phase reaction to selectively choose certain metallicity without affecting the electronic properties of nanotubes by any additive so that the residual nanotubes could be directly utilized for applications to several devices that reveal high performance. Fluorination of carbon nanotubes at relatively high temperature has been introduced to modify the electronic properties and cut the nanotube lengths.[15–19] In particular, the separation of *m*-SWCNTs from *s*-SWCNTs was not achieved with fluorination at high temperature.[19]

In this report, we have addressed a gas phase reaction in removing *m*-SWCNTs by fluorine gas in mild condition, followed by a heat treatment. The resonant Raman spectroscopy demonstrated that this process was also found to be diameter-selective as well, i.e., nanotubes with smaller diameters were removed more efficiently than those with larger diameters. The *m*-SWCNTs with small diameters were completely removed, while the counterpart *s*-SWCNTs were still retained. The effectiveness of separation at large diameters was not observed. We propose that fluorine gas induces stronger electrostatic binding between fluorine gas and *m*-SWCNT walls due to the presence of more abundant π electrons near the Fermi level compared to the counterpart *s*-SWCNTs. Thermal annealing at high temperature eventually removed the remaining *m*-SWCNTs with less than 1.1 nm.

II. EXPERIMENT

We used the raw HiPco (high-pressure CO decomposition) SWCNT powder (Carbon Nanotechnologies Inc.) for fluorination. A Ni boat filled with this powder was brought into the fluorine reaction chamber made of Ni and SUS-316 in order to prevent from erosion. The reaction process was similar to the previous report.[15,16] The chamber was pumped out to 10^{-5} bar and purged by nitrogen gases to remove the residual oxygen gases and moisture. Fluorine gas was then introduced and the pressure was maintained at 0.1 bar at room temperature for a given reaction time. After the reaction, the chamber was pumped out again to 10^{-5} bar and nitrogen gas was refilled prior to taking out the fluorinated powder sample. We note that this fluorination condition was rather mild compared to the previous works that the SWCNTs were severely disintegrated.[15,17–19] The sample was further heat-treated at 600 °C and 900 °C in Ar atmosphere.

The metallicity of samples was characterized by the resonant Raman spectroscopy (Renishaw, microprobe RM1000) with several wavelengths of 514 nm (Ar^+ ion laser), 633 nm (He-Ne laser), and 785 nm (diode laser). Samples were further analyzed by the field-emission scanning electron microscope (FESEM; JEOL 6700F). The surface chemical states of the fluorinated SWCNTs were examined by x-ray photoelectron spectroscopy (XPS) with an Electron Spectrometer PHI 5100 (VG microtech). The measurements were performed with Al-$K\alpha$ (1486.6 eV) that was operated at 300 W with a pass energy of 29.35 eV. The pressure in the analyzer chamber was 10^{-6} bar at room temperature during analysis. The instrument was calibrated using the $Ag3d_{5/2}$ line at 367.9 eV. The SWCNT powder sample was immersed in isopropanol solution and sonicated for dispersion for 4 h. The absorption spectra were obtained by dropping the solution on a quartz plate using UV-vis-NIR spectrophotometer (Hitachi U-3501). The Lorentzian function was used for the deconvolution of Raman, XPS, and absorption spectra. The parameters of the Lorentzian function were fitted to the experimental data by using the least-square method.

III. RESULTS AND DISCUSSION

Figure 1(a) shows the FESEM image of the raw HiPco SWCNTs. SWCNTs were bundled with the bundle diameter of 10–30 nm. After fluorination, the bundle size was significantly reduced, as shown in Figs. 1(b)–1(d), although a systematic change of the bundle size was not visible as a function of fluorination time. On the other hand, the sample mass was systematically increased. The increase of the sample mass was estimated as the sample mass after fluorination over the initial mass. The sample mass has already reached 170 wt. % at a reaction time of 30 minutes and 200 wt. % at 180 minutes, indicating continuous adsorption of fluorine gas on SWCNTs. This considerable mass uptake after fluorination might be due to physisorbed fluorine gas as well as covalently and semiionically bound fluorine atoms. Therefore, this increase of SWCNT mass after fluorination did not reflect the real stoichiometry, which will be discussed in XPS section. The metallicity of the sample is easily confirmed by

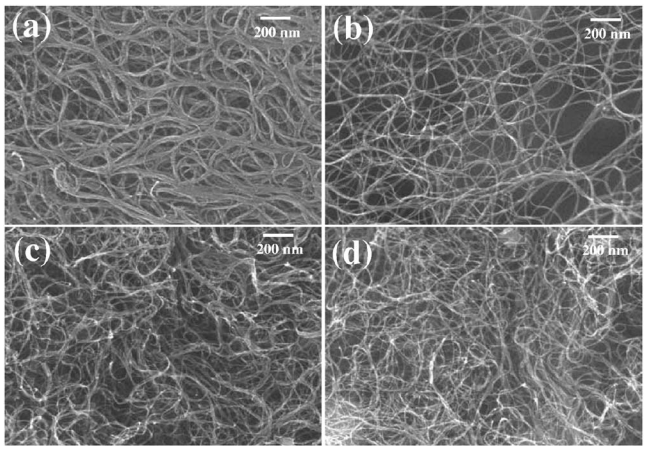

FIG. 1. Time evolution of FESEM images during fluorination: (a) the raw SWCNTs, fluorinated SWCNTs for (b) 30, (c) 60, and (d) 180 minutes.

the resonant Raman spectra. The one-dimensional nature of carbon nanotubes reveals peculiar van Hove singularities in both conduction and valence bands. The positions of van Hove singularities are strongly dependent on the chiral index (n,m). Transitions from v_i to c_i are optically allowed. The Raman signal was prominently enhanced when the excitation energy coincides with E_{ii} (transition energy from v_i to c_i). This phenomenon is called a resonant Raman. One interesting aspect is that E_{ii} is inversely proportional to the diameter and furthermore metallicity can be easily distinguished by the chiral index. This has been clearly demonstrated in Kataura plot.[20] Since some limited number of nanotubes with different chiral indices and diameters are resonant with the given excitation energy, we need several excitation energies to detect nanotubes with different diameters and chirality in the sample. We used three excitation energies in our Raman study and identified 25 SWCNTs in the raw sample, as listed in Table I.

The Raman spectrum with an excitation wavelength of 514 nm clearly shows both *s*- and *m*-SWCNTs in the radial breathing mode (RBM) of the raw SWCNTs, as shown on the left-hand panel of Fig. 2(a). The *m*-SWCNTs near 244 and 266 cm^{-1} were greatly suppressed with fluorination and completely disappeared after subsequent heat treatment. We note that the fluorination process with the subsequent annealing should be distinguished from the simple purification process from the fact that the small-diameter *m*-SWCNTs were partially etched away and remained unchanged after subsequent annealing at the same temperature, as shown in Fig. 2(b). On the other hand, *s*-SWCNTs near 183 and 204 cm^{-1} were still retained but the peak positions were slightly shifted to higher energy side after fluorination. The G peak (near 1590 cm^{-1}) of fluorinated SWCNTs was also upshifted by about 4 cm^{-1}. This peak shift is consistent with the previous report that the doping of nanotubes with halogen elements could upshift the Raman peaks by provoking the charge transfer from π electrons of nanotubes to halogen dopants.[21] This peak shift in the *s*-SWCNTs was almost recovered with heat treatment at high temperature, while maintaining their intensity ratio similar to that of the raw sample. The raw

TABLE I. Assignment of the RBMs observed with laser excitation lines of 2.41 eV, 1.96 eV, and 1.58 eV. The relative intensities of I_{raw} and I_{900} are obtained by fitting the Lorentzian line shapes on each RBM, where I_{raw} and I_{900} are the intensities of the Lorentzian peak of the raw and the heat-treated samples at 900 °C, respectively. The diameters are calculated using the formula in Ref. 25. The chiral indices (n,m) are determined using Kataura plot.

ω_{RBM} (cm^{-1})	diameter d (nm)	(n,m)	I_{raw} (%)	I_{900} (%)	Region
		E_{laser}=2.41 eV (514 nm)			
144.0(S)	1.79	(19,6) (15,11) (14,12)	3.2	0.9	III
171.4(S)	1.48	(17,3) (14,7)	12.8	4.8	III
177.7(S)	1.42	(15,5) (14,6)	10.3	13.6	III
182.3(S)	1.38	(12,8)	19.2	40.8	III
185.0(S)	1.36	(16,2)	7.4	0.6	III
205.0(S)	1.22	(15,1)	9.9	39.3	III
226.7(M)	1.10	(8,8) (12,3)	6.4	0	II
244.5(M)	1.01	(10,4)	6.7	0	II
258.8(M)	0.95	(12,0)	9.8	0	II
266.2(M)	0.92	(8,5)	13.0	0	II
308.3(S)	0.79	(10,0)	1.4	0	I
		E_{laser}=1.96 eV (633 nm)			
161.9(M)	1.58	(17,5) (13,10)	3.3	1.6	III
186.7(M)	1.35	(15,3)	3.4	7.8	III
194.3(M)	1.29	(16,1)	41.9	58.2	III
198.4(M)	1.26	(12,6)	5.6	5.0	III
218.5(M)	1.14	(11,5)	20.2	22.2	III
256.7(S)	0.98	(8,6)	21.2	5.2	II
284.1(S)	0.86	(11,0)	2.9	0	I
297.6(S)	0.82	(7,5)	1.5	0	I
		E_{laser}=1.58 eV (785 nm)			
205.1(S)	1.22	(15,1)	27.9	48.2	III
215.7(S)	1.16	(14,1)(13,3)(9,8)	6.5	8.1	III
226.2(S)	1.10	(9,7)	15.0	10.1	II
234.1(S)	1.06	(11,4)(10,5)	25.4	24.2	II
264.1(S)	0.93	(10,3)	8.2	0.6	II
267.6(S)	0.92	(11,1) (9,4)	17.0	8.8	II

SWCNTs clearly showed Breit-Wigner-Fano (BWF) resonance at the low energy side of the G-band, which is a characteristic of the *m*-SWCNTs, as shown on the right-hand panel of Fig. 2(a). The BWF line was greatly suppressed after fluorination, which is consistent with the RBM changes. The D-band near 1334 cm^{-1} was developed during fluorination and reduced significantly with heat treatment. This indicates that the fluorine molecules were adsorbed on the rest of *m*-SWCNTs and *s*-SWCNTs with large diameters during fluorination.

In order to confirm the binding nature during fluorination, we analyzed XPS spectra (Fig. 3). After fluorination, F1s XPS spectra showed a broad peak with full width at half-maximum of about 5 eV [Fig. 3(a)]. Fitted F1s XPS spectra were composed of two components near 685.5 and 687.5 eV [Fig. 3(d)]. According to previous results, F1s peaks near 685.5 and 687.5 eV were assigned to semi-ionic and covalent C-F bonds in various forms, respectively.[15,22,23] The fluorinated SWCNTs have a stoichiometry of $CF_{0.11}$, which was determined by the integrated intensity ratio of the C1s XPS peak to F1s one, adjusting for the atomic sensitivity factors of C1s and F1s. After heat treatment at 900 °C, this F1s peak completely disappeared, indicating that the fluorine molecules adsorbed on large-diameter *m*- and *s*-SWCNTs were mostly removed after heat treatment. C1s XPS spectra showed that the C-F related peak near 291 eV was also developed after fluorination [Fig. 3(b)]. The C1s peak was slightly downshifted, which is consistent with the theoretical prediction of the C-C bond weakening.[24] This is a clear evidence of chemisorption of fluorine atoms to the SWCNT walls. The F1s peak clearly disappeared and C1s peak was fully recovered to that of the raw SWCNTs after heat treatment. Thus the chemisorbed fluorine atoms provoked the charge transfer, resulting in an upshift in Raman peak posi-

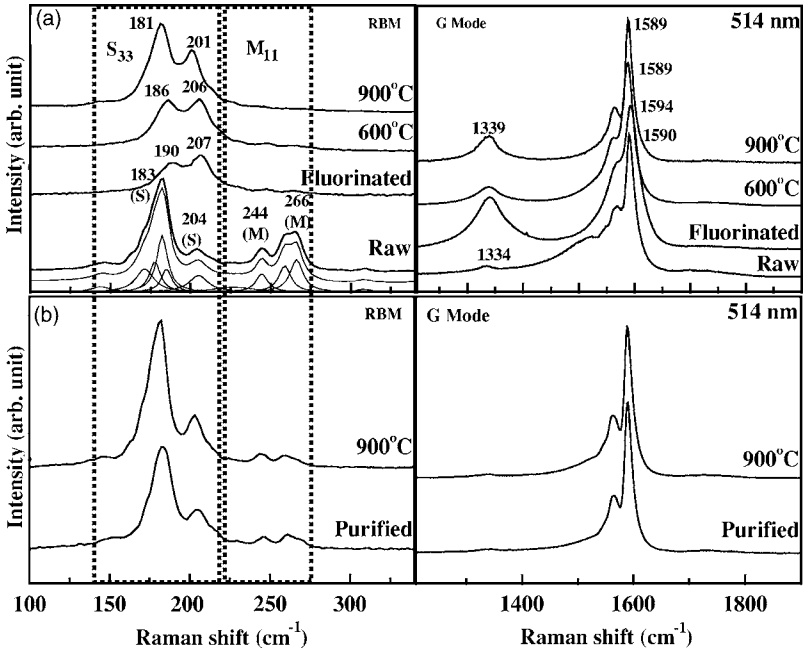

FIG. 2. Raman spectra at 514 nm excitation wavelength. (a) Left panel, RBM regions of the raw SWCNTs which was deconvoluted with several peaks (Lorentzian), fluorinated SWCNTs for 30 minutes, and fluorinated SWCNTs followed by the heat treatment at 600 °C and 900 °C from the bottom spectrum. The box indicates the range of semiconducting and metallic components determined from Kataura plot. Right panel, G-band regions with same notations to the RBMs. (b) Raman spectra of the purified SWCNTs for comparison.

tion, and further disintegrated the *m*-SWCNT walls selectively, which was evidenced by a diminution of BWF lines [Fig. 2(a)]. On the other hand, the *s*-SWCNTs were retained without pronounced changes. The raw sample also contained oxygen atoms that were both physisorbed and chemisorbed [Fig. 3(c)]. The amount of oxygen content was increased during fluorination. Some oxygen atoms were still left in the sample after heat treatment at 900 °C. Strongly chemisorbed oxygen atoms could be retained at the defects located at the walls or edges of SWCNTs.

Figure 4 shows resonant Raman spectra at different excitation energies. The RBM peaks with an excitation wavelength of 785 nm revealed the dominant *s*-SWCNTs near 205, 226, 234, and 267 cm^{-1} with the corresponding diam-

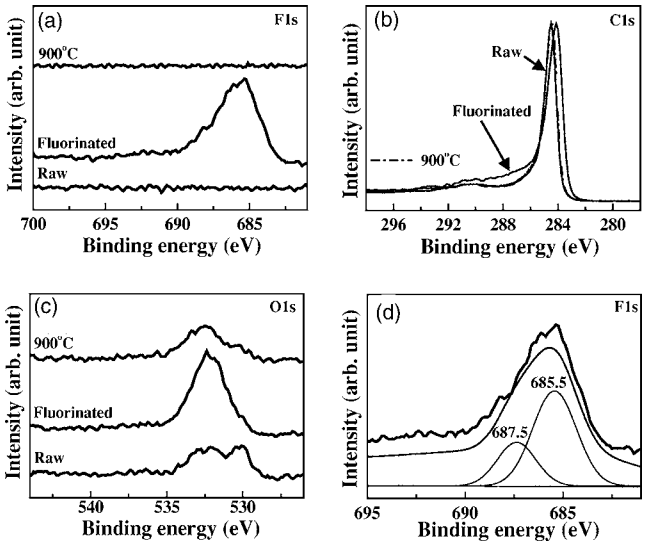

FIG. 3. (a) F1s, (b) C1s, and (c) O1s XPS spectra for the raw SWCNTs, the fluorinated SWCNTs for 30 minutes, and heat-treated (900 °C) SWCNTs after fluorination. (d) Deconvoluted F1s XPS spectra for fluorinated SWCNTs.

eters of 1.22, 1.10, 1.06, and 0.92 nm, respectively [Fig. 4(a)].[25] The RBM peaks of the *s*-SWCNTs and G peak did not show appreciable peak shifts even after fluorination. We note that the peak intensities of the *s*-SWCNTs with smaller diameters were diminished more prominently. Yet the *s*-SWCNTs with small diameters less than 1.1 nm were still retained without peak shift after heat treatment, in good contrast with the small-diameter *m*-SWCNTs that were removed even after heat treatment, as shown in Fig. 2(a). The similar changes have been observed in the RBM of Raman spectra with an excitation wavelength of 633 nm [Fig. 4(b)]. In this case, however, all the SWCNTs with diameters less than 0.9 nm were removed regardless of the metallicity. Considerable amount of *s*-SWCNTs with diameters ranging from 0.9 to 1.1 nm were still retained. Peaks from *m*-SWCNTs with large diameters seemed to be suppressed during fluorination but these peaks were recovered after heat treatment. The selectivity was not observed particularly at SWCNTs with large diameters. Our results showed clear diameter-dependent selectivity. Careful tuning of fluorination reaction condition is required to improve the selectivity.

Figure 5 shows a detailed analysis of the deconvoluted G-bands, which were fitted using BWF and Lorentzian lines. The G-band is composed of six components.[26] The existence of the broad BWF line (at 1524 cm^{-1}) at a lower energy side of the G-band with an excitation wavelength of 514 nm indicates clearly abundance of *m*-SWCNTs in the raw sample. The BWF line was completely removed after fluorination followed by heat treatment. This clearly shows that the *m*-SWCNTs with smaller diameters were completely removed, while most of the semiconducting components were retained. As a result, $|1/q|$ was zero after annealing fluorinated SWCNTs, suggesting disappearance of the BWF resonance.[26] In general, the metallicity of SWCNTs is related to the absolute value of the fitting parameter $1/q$ that is a measure of the interaction of the phonon with a continuum of states. We also found that the XPS spectra showed a significant reduction in the density of states of the valence band

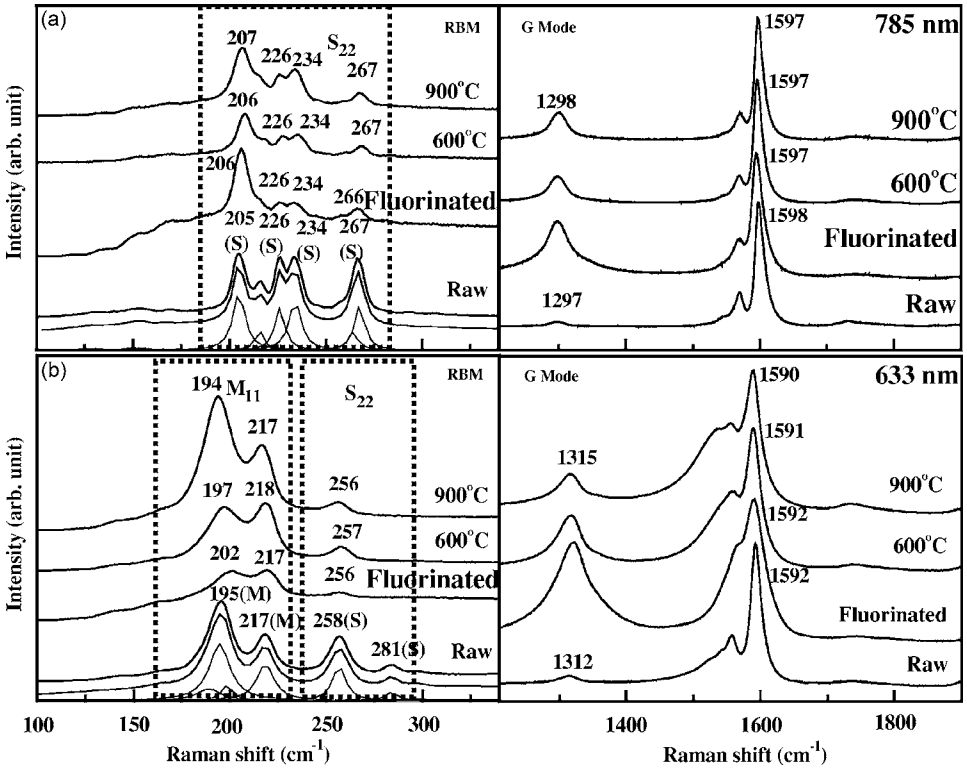

FIG. 4. RBM (left panel) and G-band (right panel) regions in Raman spectra at different excitation wavelengths, (a) 785 nm and (b) 633 nm.

near the Fermi level after fluorination. The decrease of the density of states was more severe after heat treatment (not shown here). This implies that the *m*-SWCNTs were removed appreciably after fluorination followed by heat treatment.

Although the resonant Raman spectra are advantageous in determining metallicity of the individual SWCNTs, it does not provide information for metallicity of the whole sample. The metallicity of the whole sample can be shown in the absorption spectra, as shown in Fig. 6. The raw sample clearly showed S_{11}, S_{22}, and M_{11} transitions between van Hove singularities in the valence band and conduction band. Although several subband peaks were observed in each band, the incomplete nanodispersion of SWCNTs in isopropanol solution obscured a comprehensive analysis with these peaks.[27] These bands, however, were significantly altered after fluorination and subsequent heat treatment. We note that the M_{11} peaks disappeared except for the peak at the lower energy side, again indicating that *m*-SWCNTs with small diameters were removed in the sample. These results are consistent with diameter-selective removal of *m*-SWCNTs observed in the Raman spectra. Since the S_{11} band can be easily modified by the environment,[28] the separation yield of the sample can be drawn by the intensity ratio of S_{22} and M_{11} bands of the optical absorption spectra.[12,13] The composition of *s*-SWCNTs, $S_{22}/(S_{22}+M_{11})$, was 0.63 from the raw sample, which is close to the theoretical value of 0.67. This was increased to 0.86 after fluorination and subsequent heat treatment.

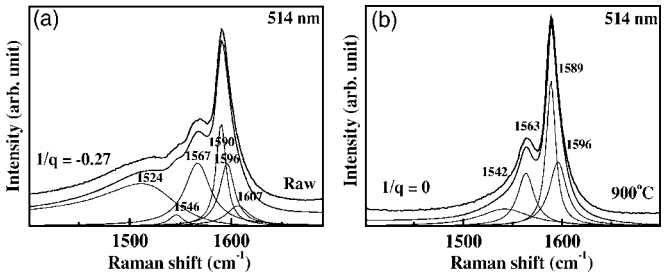

FIG. 5. Deconvolution of the G-band for (a) the raw SWCNTs and (b) the heat-treated SWCNTs after fluorination for 30 minutes: excitation wavelengths of 514 nm. The line at 1524 cm^{-1} indicates the BWF line shape of *m*-SWCNTs. The metallic and semiconducitng peaks were fitted using BWF and Lorentzian lines. The asymmetric BWF line shape is described by $I(\omega)=I_0\{[1+(\omega-\omega_{\mathrm{BWF}})/q\Gamma]^2/1+[(\omega-\omega_{\mathrm{BWF}})/\Gamma]^2\}$, where $1/q$ is a measure of the interaction of the phonon with a continuum of states, and ω_{BWF} is the BWF peak frequency at maximum intensity I_0 (Ref. 26).

Although we observed selectivity in removing *m*-SWCNTs using fluorine gas attack, it is not so obvious how this could work. Fluorine molecule approaches the nanotube wall and is dissociatively chemisorbed. The energy gain after chemisorption is about −5 eV for both *m*- and *s*-SWCNTs.[23] The preferable energy gain for *m*-SWCNTs could be negligible compared to large chemisorption energy. We note that the degree of fluorination is strongly dependent on the reaction temperature.[15] The SWCNTs were seriously damaged at a reaction temperature of 200 °C.[15] Therefore the selective reaction is kinetics limited and should occur during chemisorption process. When fluorine molecule is first physisorbed, no significant charge transfer will occur but a slightly larger energy gain could be expected in the *m*-SWCNTs by the image potential of the induced dipole interactions. As the fluorine molecule approaches closer to the tube, the F-F bond becomes weaker and the amount of charge transfer from nanotube to the fluorine molecule will be increased. The availability of the charge density at the

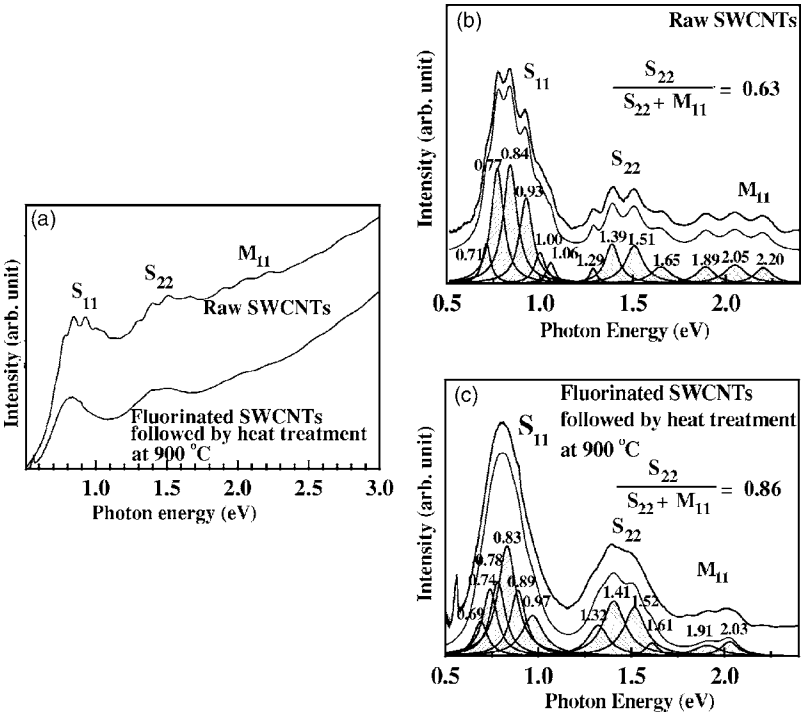

FIG. 6. (a) Absorption spectra of the raw SWCNTs (upper line) and the fluorinated SWCNTs for 30 minutes followed by heat treatment (bottom line). Curve fitting of the S_{22} and M_{11} bands after subtraction of the plasmon baseline for (b) the raw SWCNTs and (c) the heat-treated SWCNTs after fluorination for 30 minutes.

Fermi level of the nanotubes is the key factor to give selectivity of adsorption. More charge transfer is expected from *m*-SWCNTs due to the abundant electron density at the Fermi level. At a transition state, the maximum charge transfer is expected and therefore the difference in the adsorption energy between *m*- and *s*-SWCNTs will be maximized as well. In other words, the barrier height in the transition state should be lower in the *m*-SWCNTs. The difference in the barrier height can be estimated to be about 0.5 eV or less. We also propose that this charge transfer assists the nanotube bundle to be debundled by the electrostatic repulsion between nanotubes during the reaction so that other approaching fluorine molecules could be intercalated more efficiently. Otherwise, the *m*-SWCNTs located inside the bundle cannot be removed. A better yield of separation is expected if one begins with nanodispersed SWCNTs.

IV. CONCLUSION

We have investigated a gas phase reaction using fluorine gas to selectively remove *m*-SWCNTs from mixture of *m*- and *s*-SWCNTs. We summarize our findings as follows. No fluorine atoms were left in the sample after fluorination followed by heat treatment at 900 °C.

(1) The fluorine gas was strongly chemisorbed or (semi) ionic bonded during fluorination, which was confirmed by the increased mass after fluorination and XPS spectra. SWCNTs were dissociated during fluorination and further disintegrated in a form of CF_n gas during the following heat treatment.

(2) Adsorption and desorption of fluorine atoms were monitored by the peak shift of the RBMs in the Raman spectra.

(3) The yield of selective removal of *m*-SWCNTs was diameter dependent. In region I with diameters less than 0.9 nm, both *s*- and *m*-SWCNTs were removed completely. In region II with diameters ranging from 0.9 to 1.1 nm, all the *m*-SWCNTs were removed with high selectivity. In region III with diameters greater than 1.1 nm, the selectivity became less obvious. This indicates that the selective adsorption was promoted by the strain.

(4) The charge transfer from SWCNTs to fluorine atoms plays a key role in determining the selective adsorption. Larger charge transfer is expected from *m*-SWCNTs due to more abundant electron density at the Fermi level compared to the counterpart *s*-SWCNTs. We propose that the adsorption barrier height should be lower in the *m*-SWCNTs, giving easier accessibility to *m*-SWCNTs during adsorption.

ACKNOWLEDGMENTS

This research was supported by Grant No. 05K1401-00412 from Center for Nanoscale Mechatronics and Manufacturing and TND project, one of the 21st Century Frontier Research Programs, which are supported by Ministry of Science and Technology in Korea, and CNNC at SKKU.

*Author to whom correspondence should be addressed. Electronic address: leeyoung@skku.edu

[1] R. Saito, M. Fujita, G. Dresselhaus, and M. S. Dresselhaus, Appl. Phys. Lett. **60**, 2204 (1992).

[2] N. Hamada, S. I. Sawada, and A. Oshiyama, Phys. Rev. Lett. **68**, 1579 (1992).

[3] S. Iijima and T. Ichibashi, Nature (London) **363**, 603 (1993).

[4] D. S. Bethune, C. H. Kiang, M. S. de Vries, G. Gorman, R.

Savoy, J. Vazquez, and R. Berers, Nature (London) **363**, 605 (1993).
[5] A. Thess, R. Lee, P. Nikolaev, H. Dai, P. Petit, J. Robert, C. Xu, Y. H. Lee, S. G. Kim, A. G. Rinzler, D. T. Colbert, G. E. Scuseria, D. Toman, J. E. Fischer, and R. E. Smalley, Science **273**, 483 (1996).
[6] P. Nikolaev, M. J. Bronikowski, R. K. Bradley, F. Rohmund, D. T. Colbert, K. A. Smith, and R. E. Smalley, Chem. Phys. Lett. **313**, 91 (1999).
[7] S. J. Tans, A. R. M. Verschueren, and C. Dekker, Nature (London) **393**, 49 (1998).
[8] D. Chattopadhyay, I. Galeska, and F. Papadimitrakopoulos, J. Am. Chem. Soc. **125**, 3370 (2003).
[9] R. Krupke, F. Hennrich, H. v. Löhneysen, M. Manfred, and M. M. Kappes, Science **301**, 344 (2003).
[10] M. Zheng, A. Jagota, M. S. Strano, A. P. Santos, P. Barone, S. G. Chou, B. A. Diner, M. S. Dresselhaus, R. S. Mclean, G. B. Onoa, G. G. Samsonidze, E. D. Semke, M. Usrey, and D. J. Walls, Science **302**, 1545 (2003).
[11] H. Li, B. Zhou, Y. Lin, L. Gu, W. Wang, K. A. Shiral Fernando, S. Kumar, L. F. Allard, and Y. P. Sun, J. Am. Chem. Soc. **126**, 1014 (2004).
[12] C.-M. Yang, J. S. Park, K. H. An, S. C. Lim, K. Seo, B. Kim, K. A. Park, S. Han, C. Y. Park, and Y. H. Lee, J. Phys. Chem. B **109**, 19242 (2005).
[13] K. H. An, J. S. Park, C.-M. Yang, S. Y. Jeong, S. C. Lim, C. Kang, J.-H. Son, M. S. Jeong, and Y. H. Lee, J. Am. Chem. Soc. **127**, 5196 (2005).
[14] K. Y. Seo, C. W. Kim, Y. S. Choi, K. A. Park, Y. H. Lee, and B. S. Kim, J. Am. Chem. Soc. **125**, 13946 (2003).
[15] K. H. An, J. G. Heo, K. K. Jeon, D. J. Bae, C. W. Yang, C. Y. Park, and Y. H. Lee, Appl. Phys. Lett. **80**, 4235 (2002).
[16] K. H. An, K. A. Park, J. G. Heo, J. Y. Lee, K. K. Jeon, S. C. Lim, C. W. Yang, Y. S. Lee, and Y. H. Lee, J. Am. Chem. Soc. **125**, 3057 (2003).
[17] E. T. Mickelson, C. B. Huffman, A. G. Rinzler, R. E. Smalley, R. H. Hauge, and J. L. Margrave, Chem. Phys. Lett. **296**, 188 (1998).
[18] Z. Gu, H. Peng, R. H. Hauge, R. E. Smalley, and J. L. Margrave, Nano Lett. **2**, 1009 (2002).
[19] P. E. Pehrsson, W. Zhao, J. W. Baldwin, C. Song, J. Liu, S. Kooi, and B. Zheng, J. Phys. Chem. B **107**, 5690 (2003).
[20] H. Kataura, Y. Kumazawa, Y. Maniwa, I. Umezu, S. Suzuki, Y. Ohtsuka, and Y. Achiba, Synth. Met. **103**, 2555 (1999).
[21] A. M. Rao, P. C. Eklund, S. Bandow, A. Thess, and R. E. Smalley, Nature (London) **388**, 257 (1997).
[22] Y. Hattori, H. Kanoh, F. Okino, H. Touhara, D. Kasuya, M. Yudasaka, S. Iijima, and K. Kaneko, J. Phys. Chem. B **108**, 9614 (2004).
[23] N. Watanabe, T. Nakajima, and H. Touhara, *Graphite Fluorides* (Elsevier, Amsterdam, 1988).
[24] K. A. Park, Y. S. Choi, Y. H. Lee, and C. Kim, Phys. Rev. B **68**, 045429 (2003).
[25] We used the following formula, $\omega_{\mathrm{RBM}}=233/d_t+14$, RMS=1.99, from Ch. Kramberger, R. Pfeiffer, H. Kuzmany, V. Zolyomi, and J. Kurti, Phys. Rev. B **68**, 235404 (2003).
[26] S. D. M. Brown, A. Jorio, P. Corio, M. S. Dresselhaus, G. Dresselhaus, R. Saito, and K. Kneipp, Phys. Rev. B **63**, 155414 (2001).
[27] M. J. O'Connell, S. M. Bachilo, C. B. Huffman, V. C. Moore, M. S. Strano, E. H. Haroz, K. L. Rialon, P. J. Boul, W. H. Noon, C. Kittrell, J. Ma, R. H. Hauge, R. B. Weisman, and R. E. Smalley, Science **297**, 593 (2002).
[28] M. E. Itkis, D. E. Perea, S. Niyogi, S. M. Rickard, M. A. Hamon, H. Hu, B. Zhao, and R. C. Haddon, Nano Lett. **3**, 309 (2003).